Supplementary Information for

Effect of near-field optical angular momentum on molecular junctions

Jianchen Zi[1], Michaël Lobet[2], Luc Henrard[2], Zhiqiang Li[1], Chenhui Wang[1], Xiaohong Wu[3], Hai Bi[1]*

[1] *Jihua Laboratory, No.28 Huandao South road, Nanhai district, Foshan 528200, China*
[2] *Department of Physics and Namur Institute of Structured Materials, University of Namur, Rue de Bruxelles 61, 5000 Namur, Belgium*
[3] *MIIT Key Laboratory of Critical Material Technology for New Energy Conversion and Storage, School of Chemistry and Chemical Engineering, Harbin Institute of Technology, Harbin 150001, China*

SI.1 Density Functional Theory.

All DFT calculations performed in this study adopt B3LYP method including Grimme's dispersion (D3BJ) correction in conjunction with 6-31G(d,p) basis set by Gaussian 09 D.01 package. The stationary-state geometry was used as an input for relaxed scan of potential energy surface. During the relaxed scan, the torsion angles of the middle and two peripheral phenylene rings changed. After the relaxed scan, vibration analyses were computed for each step of the relaxed scan. Since the vibration analyses were carried out under harmonic approximation, a fundamental scale factor of 0.9627 pre-fitted for B3LYP/6-31G(d,p) level was applied for all calculated frequencies to relieve overestimations of vibrational frequencies[1]. The data of vibration analysis of Gaussian were converted into Raman spectra using the Multiwfn code[2] by employing the Lorentzian broadening function with full width at half maximum (FWHM) of 8 cm^{-1}. The Raman spectra were simulated based on the Raman intensities derived by the following equation[3]

$$I_i = \frac{C(v_0 - v_i)^4 S_i}{v_i B_i}; \quad B_i = 1 - \exp\left(-\frac{hcv_i}{k_\text{B}T}\right) \tag{S1}$$

where i denotes vibrational mode, C is normalization factor that can be arbitrarily chosen, h, c, and k_B are Planck constant, light speed, and Boltzmann constant, respectively; S_i is Raman activity given by Gaussian, v_i is vibrational frequency, v_0 corresponds to frequency of incident light, T is set as 298.15 K.
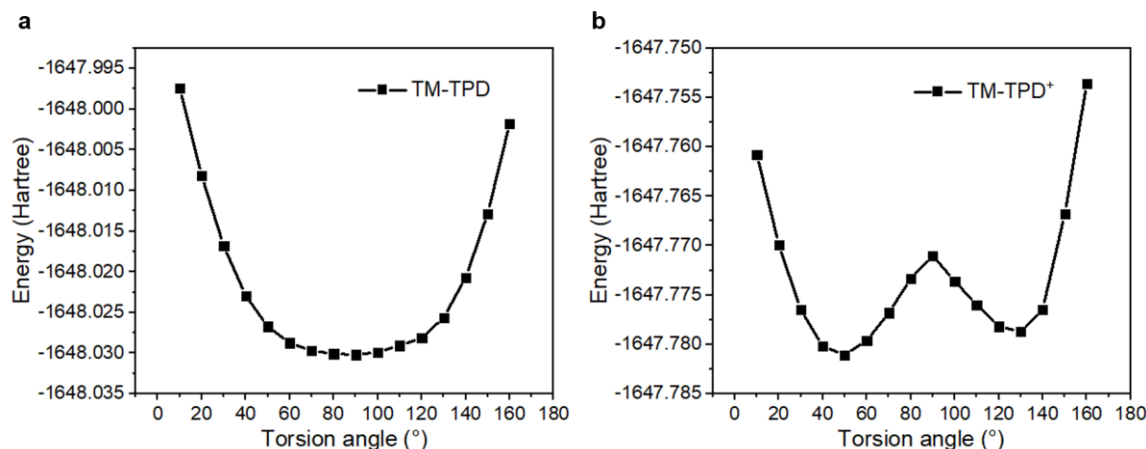
Figure S1: **Potential energy curve of isolated TM-TPD molecule.** a and b are the potential energy curves of neutral and positively charged TM-TPD molecule, respectively. Relaxed scans along the torsion angles of the middle phenylene ring and peripheral phenylene ring with a step size of 10°. The two peripheral phenylene rings were rotated synchronously.

As shown in Figure S1, the energy change of the TM-TPD molecule caused by the change of dihedral angle defined as the torsion angle of middle phenylene ring and peripheral phenylene ring is relatively small, and is smaller than 0.03 hartree between 30° to 140°. The neutral TM-TPD has the lowest potential energy at 90°, while the charged has two local minimums at 50° and 130°. The charged molecules with the torsion angle of 50° and 130° have identical conformations and effects, thus we just consider the case of 50°. The vibration characteristics for each mode retaliated to Raman spectrum peaks are shown in Figure S2. The vibrational modes around 1272 cm^{-1}, 1391 cm^{-1}, 1467 cm^{-1} and 1568 cm^{-1} mainly correspond to the stretching vibration of single bond between the middle and two peripheral phenylene rings, breathing vibration of peripheral phenylene ring, stretching vibration of middle phenylene ring, and stretching vibration of peripheral phenylene rings. When conducting, the torsion angle changed from 90° (OFF mode) to 50° (ON mode), and TM-TPD molecule tends to be better conjugated. The conjugated electrons of the phenylene rings tend to be shared by the single bonds between the phenylene rings, thus enhance the Raman activity of the molecule.

1272 cm⁻¹

1391 cm⁻¹

1467 cm⁻¹

1568 cm⁻¹
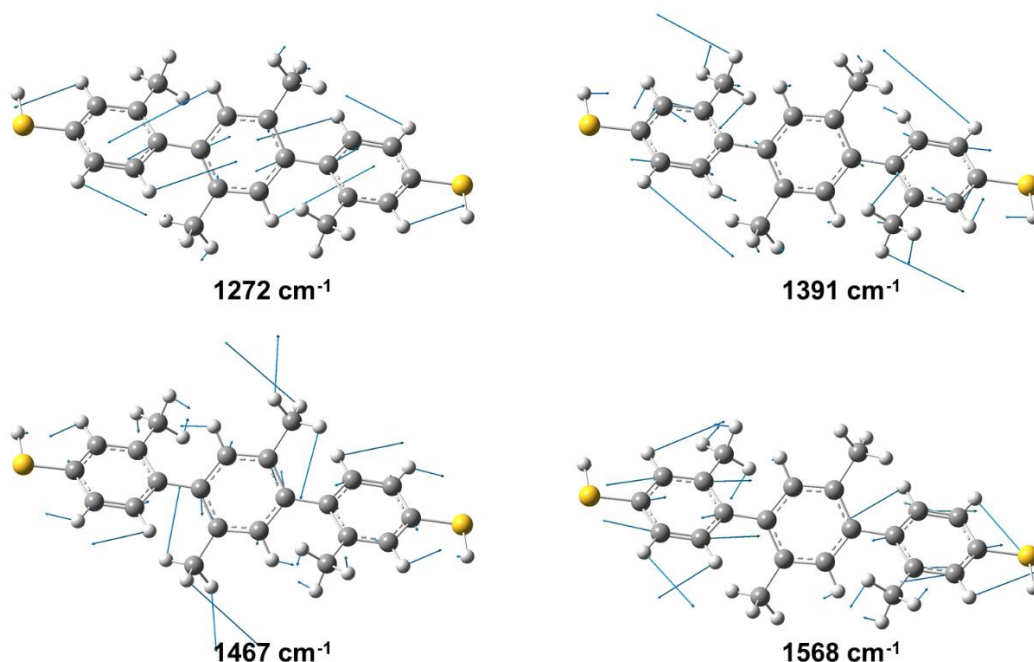
Figure S2: **The vibration characteristics for positively charged TM-TPD molecule with a torsion angle of 40° of specific mode.**

SI.2 Near-field modes for side illumination with different nanostructures.
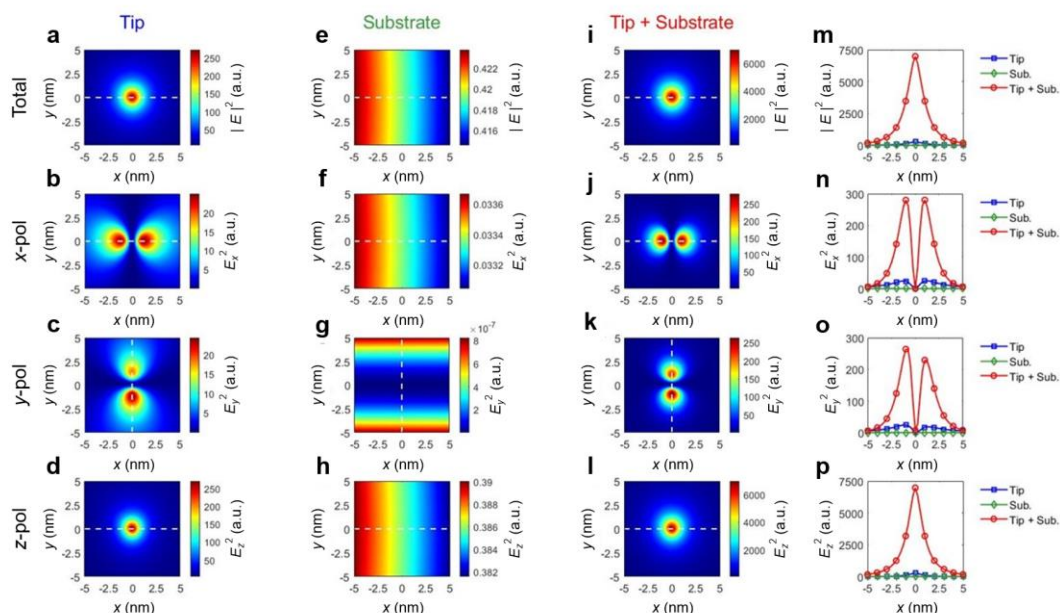
Figure S3: **Electric field intensity distributions of near-field mode for side illumination with different nano structures.** The total and components of electric field intensity distribution are shown in $z = 0$ plane for (a-d) tip only, (e-h) substrate only, (i-l) tip with substrate. (m-p) Profiles of the electric field intensity at $y = 0$ or $x = 0$ (white dash lines).

Using p-polarised light sent from the left side, we computed the total and components of near-field intensity for side illumination with different nano structures, as shown in Figure S3. The main contributor to the intensity is the E_z component. The combination of both the tip and the substrate is essential to confine light tightly. The tip-structure can excite a local surface plasmon (LSP) mode, while the substrate cannot excite a LSP mode. However, the combination of tip and substrate brings a great improvement on the near-field excitation.

SI.3 Analysis of near-field mode symmetry for top p-(s-)polarised illumination with TP tip.

For top p-(s-)polarised illumination with the TP tip, we can study the electromagnetic near-field using the symmetry of optical system. The gap-structure here is mirror symmetric along x-axis. The electric field in the optical system can be defined as

$$\vec{E} = \begin{bmatrix} E_x \\ E_y \\ E_z \end{bmatrix} \tag{S2}$$

When the electric field is mirror symmetric along x-axis, we can get

$$\begin{bmatrix} E_x(x) \\ E_y(x) \\ E_z(x) \end{bmatrix} = \begin{bmatrix} -E_x(-x) \\ E_y(-x) \\ E_z(-x) \end{bmatrix} \tag{S3}$$

Consequently, the E_x must be suppressed at $x = 0$ as

$$E_x(0) = 0 \tag{S4}$$

When the electric field is mirror antisymmetric along x-axis, we can get

$$\begin{bmatrix} E_x(x) \\ E_y(x) \\ E_z(x) \end{bmatrix} = \begin{bmatrix} E_x(-x) \\ -E_y(-x) \\ -E_z(-x) \end{bmatrix} \tag{S5}$$

Then, E_y and E_z are suppressed at $x = 0$ as

$$\begin{cases} E_y(0) = 0 \\ E_z(0) = 0 \end{cases} \tag{S6}$$

Obviously, the top p-polarised illumination brings a mirror antisymmetry of electric field along x-axis, thus the E_z at $x = 0$ is zero and suppressed the generation of gap-mode which relies on the E_z, while the top s-polarised illumination has little suppression of the gap-mode due to its mirror symmetric of electric field.

SI.4 Analysis of near-field AMD symmetry for top s-polarised illumination with TP tip.

According to Equation 1, the components of AMD can be expressed as

$$\begin{bmatrix} l_x \\ l_y \\ l_z \end{bmatrix} = \varepsilon\mu \left(\begin{bmatrix} r_x \\ r_y \\ r_z \end{bmatrix} \times \begin{bmatrix} S_x \\ S_y \\ S_z \end{bmatrix} \right) = \varepsilon\mu \begin{bmatrix} r_y S_z - r_z S_y \\ r_z S_x - r_x S_z \\ r_x S_y - r_y S_x \end{bmatrix} \tag{S7}$$

Moreover, the components of Poynting vector can be expressed as

$$\begin{bmatrix} S_x \\ S_y \\ S_z \end{bmatrix} = \frac{1}{2}\text{Re} \left(\begin{bmatrix} E_x \\ E_y \\ E_z \end{bmatrix} \times \begin{bmatrix} H_x^* \\ H_y^* \\ H_z^* \end{bmatrix} \right) = \frac{1}{2}\text{Re} \left(\begin{bmatrix} E_y H_z^* - E_z H_y^* \\ E_z H_x^* - E_x H_z^* \\ E_x H_y^* - E_y H_x^* \end{bmatrix} \right) \tag{S8}$$

In the case of top s-polarised illumination with the TP tip, the $\vec{E}$ and tip-structure are symmetric along x-axis, but the $\vec{H}$ is antisymmetric, thus the optical system satisfies the following conditions as

$$\begin{cases} \begin{bmatrix} E_x(x) \\ E_y(x) \\ E_z(x) \end{bmatrix} = \begin{bmatrix} -E_x(-x) \\ E_y(-x) \\ E_z(-x) \end{bmatrix} \\ \begin{bmatrix} H_x(x) \\ H_y(x) \\ H_z(x) \end{bmatrix} = \begin{bmatrix} H_x(-x) \\ -H_y(-x) \\ -H_z(-x) \end{bmatrix} \\ \begin{bmatrix} r_x(x) \\ r_y(x) \\ r_z(x) \end{bmatrix} = \begin{bmatrix} -r_x(-x) \\ r_y(-x) \\ r_z(-x) \end{bmatrix} \end{cases} \tag{S9}$$

— 5 —

We can get

$$
\begin{bmatrix} S_x(x) \\ S_y(x) \\ S_z(x) \end{bmatrix} = \frac{1}{2}\mathrm{Re}\left(\begin{bmatrix} E_y(x)H_z^*(x) - E_z(x)H_y^*(x) \\ E_z(x)H_x^*(x) - E_x(x)H_z^*(x) \\ E_x(x)H_y^*(x) - E_y(x)H_x^*(x) \end{bmatrix}\right)
$$
$$
= \frac{1}{2}\mathrm{Re}\left(\begin{bmatrix} E_z(-x)H_y^*(-x) - E_y(-x)H_z^*(-x) \\ E_z(-x)H_x^*(-x) - E_x(-x)H_z^*(-x) \\ E_x(-x)H_y^*(-x) - E_y(-x)H_x^*(-x) \end{bmatrix}\right) = \begin{bmatrix} -S_x(-x) \\ S_y(-x) \\ S_z(-x) \end{bmatrix} \tag{S10}
$$

and further

$$
\begin{bmatrix} l_x(x) \\ l_y(x) \\ l_z(x) \end{bmatrix} = \varepsilon\mu\begin{bmatrix} r_y(x)S_z(x) - r_z(x)S_y(x) \\ r_z(x)S_x(x) - r_x(x)S_z(x) \\ r_x(x)S_y(x) - r_y(x)S_x(x) \end{bmatrix}
$$
$$
= \varepsilon\mu\begin{bmatrix} r_y(-x)S_z(-x) - r_z(-x)S_y(-x) \\ r_x(-x)S_z(-x) - r_z(-x)S_x(-x) \\ r_y(-x)S_x(-x) - r_x(-x)S_y(-x) \end{bmatrix} = \begin{bmatrix} l_x(-x) \\ -l_y(-x) \\ -l_z(-x) \end{bmatrix} \tag{S11}
$$

It states that the AMD is antisymmetric along *x*-axis in the system.

SI.5 Additional Experimental Procedures.

A. Molecular Junction Spectroscopy Instrument.

Molecular junction spectroscopy (MJS, Figure 1) enables simultaneous current-voltage (*I-V*) and optical spectroscopy measurements in single molecules contacted by atomically sharp electrodes. The experiments were performed in a home-built set-up[4-5]. The employed thiol-terminated species were anchored to a gold film and contacted from the other side by the apex of a gold-covered (20 nm) tetrahedral glass fragment. The tip acted as the light source, counter electrode, and light collector at the same time. The tip-sample distance was controlled by a piezo. A He-Ne laser (12 mW, 632.8 nm) and a SpectraPro 2310i monochromator were employed for high-resolution Raman spectroscopy measurements. Near-field Raman spectroscopy was achieved by using an objective with a high numerical aperture (Olympus, NA = 0.8, WD 3.4 mm) for both focusing and collecting the back scattered light from the molecular junction. The laser spot with a radius of ~5 µm was focused through the backside of a gold-coated (20 nm) tetrahedral glass

fragment, into the apex of the tip. All measurements shown in the main text were recorded in high vacuum ($\sim 1 \times 10^{-7}$ mbar).

B. Substrate Preparation.

The clean glass slide was coated with a 200−500 nm gold film by thermal evaporation. A droplet of the molecular solution (0.5 mM) of TM-TPD in tetrahydrofuran (THF, Aldrich) was deposited with a pipet on the gold-covered substrate. Then the substrate was put in an atmosphere saturated with the THF solvent for 3 h, which affords a dilute layer with the molecules covalently anchored to the substrate.

C. Molecular Junction Preparation.

The substrate was prepared exsitu and fixed on the sample holder in the vacuum chamber. The tip was approached mechanically into the working distance of the piezo crystal with the help of a tunneling current feedback loop. To establish a molecular junction, the sample was approached with $V_{sample} = 0.5$ V to the tip repeatedly until the current jumps out of tunneling, typically between $I = 1 \times 10^{-9}$ and 1×10^{-7} A. When stable $I-V$ curves were found, the Raman spectra were recorded.

D. Conductance with side and top illumination
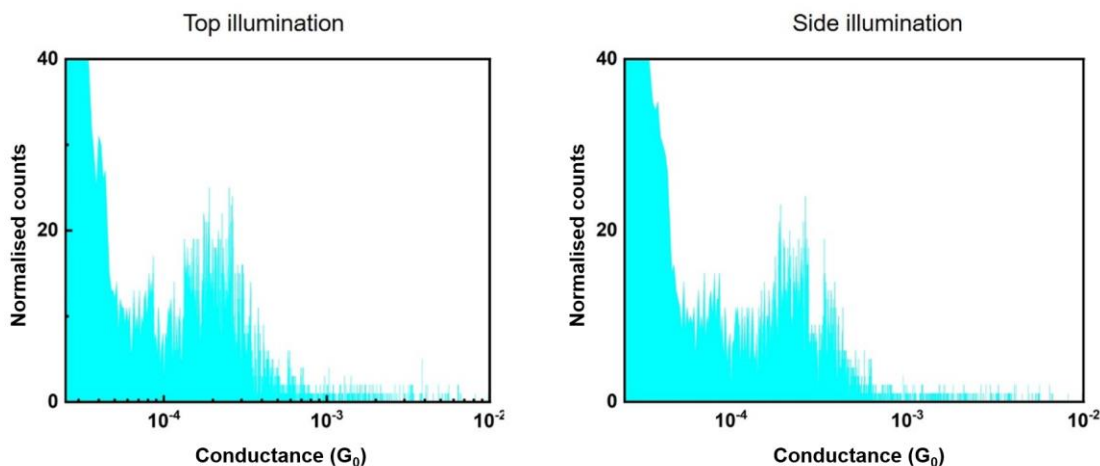
Figure S4: **Electrical conductance of charged TM-TDM molecular junctions under top and side illumination.**

The electrical conductance of the TM-TDM molecular junctions under top and side illumination were measured and shown in Figure S4. Typical current histograms of OPE-3 do not depend on the illumination geometry. Typical conductance of the molecular

junction was measured under 1.0 V. The rotational vibration of the molecules does not significantly change the conductance.

E. Reproducibility of experimental results

For top and side illumination, 5 groups of measurements are shown in Figure S5.
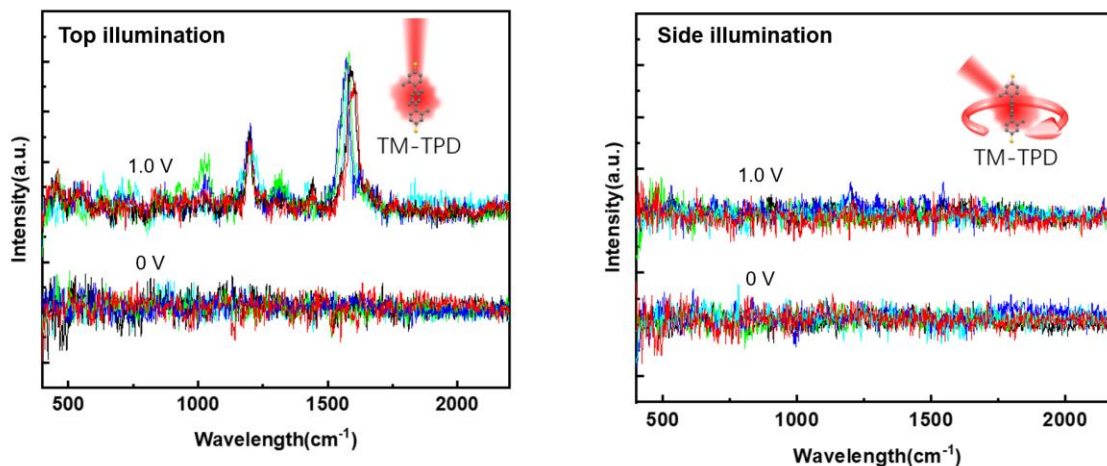
Figure S5:   Reproducibility test of experimental results.

Reference

1.   Merrick, J. P.; Moran, D.; Radom, L., An evaluation of harmonic vibrational frequency scale factors. *J Phys Chem A* **2007,** *111* (45), 11683-700.

2.   Lu, T.; Chen, F., Multiwfn: a multifunctional wavefunction analyzer. *J. Comput. Chem.* **2012,** *33* (5), 580-92.

3.   Michalska, D.; Wysokiński, R., The prediction of Raman spectra of platinum(II) anticancer drugs by density functional theory. *Chemical Physics Letters* **2005,** *403* (1-3), 211-217.

4.   Bi, H.; Palma, C. A.; Gong, Y.; Hasch, P.; Elbing, M.; Mayor, M.; Reichert, J.; Barth, J. V., Voltage-Driven Conformational Switching with Distinct Raman Signature in a Single-Molecule Junction. *J. Am. Chem. Soc.* **2018,** *140* (14), 4835-4840.

5.   Bi, H.; Lobet, M.; Saikin, S. K.; Li, Y.; Huo, C.; Jian, J.; Wu, X.; Reichert, J.; Aspuru-Guzik, A.; Mazur, E., Optically Induced Molecular Logic Operations. *ACS Nano* **2020,** *14* (11), 15248-15255.